SUPPORTING INFORMATION

The impact of spin-orbit coupling on fine-structure and spin polarisation in photoexcited triplet state palladium porphyrins

Gabriel Moise,*†,(a) Ashley J. Redman,†,(a) Sabine Richert,(a,b) William K. Myers,(a) Ibrahim Bulut,(c) Pernille S. Bolls,(c) Michel Rickhaus,(c) Jibin Sun,(c) Harry L. Anderson,*(c) and Christiane R. Timmel*(a)

(*a*) *Centre for Advanced Electron Spin Resonance (CAESR), Inorganic Chemistry Laboratory, Department of Chemistry, University of Oxford, South Parks Road, Oxford OX1 3QR, United Kingdom.*

(*b*) *Institute of Physical Chemistry, University of Freiburg, Albertstraße 21, 79104 Freiburg, Germany.*

(*c*) *Chemistry Research Laboratory, Department of Chemistry, University of Oxford, 12 Mansfield Road, Oxford OX1 3TA, United Kingdom.*

† *These authors contributed equally.*

* *Corresponding authors:*
gabriel.moise@physics.ox.ac.uk
harry.anderson@chem.ox.ac.uk
christiane.timmel@chem.ox.ac.uk

Contents

1 Synthesis and characterisation of dimers

1.1 General remarks

All reagents were purchased from commercial sources and solvents were used as supplied. ^{1}H-NMR data were recorded at 400 MHz using a Bruker AVII400 or AVIII400 at 298 K. Chemical shifts are quoted as parts per million (ppm) relative to residual $CHCl_3$ (δ_H = 7.26 ppm). Multiplicity (s = singlet, d = doublet, t = triplet, and m = multiplet) and coupling constants (J) in Hz are reported whenever possible. MALDI-ToF spectra were measured at the EPSRC National Mass Spectrometry service (Swansea) using a Bruker MicroflexTM LRF. UV-vis-NIR absorbance measurements were recorded at 25 °C with a Perkin-Elmer Lambda 20 photospectrometer using 1 cm silica cuvettes.

1.2 Experimental procedures for synthesis of porphyrin dimers

The bis-zinc dimer, compound **Zn_2**, was synthesized as reported previously.[1,2]

Synthesis of Fb_2 and ZnFb

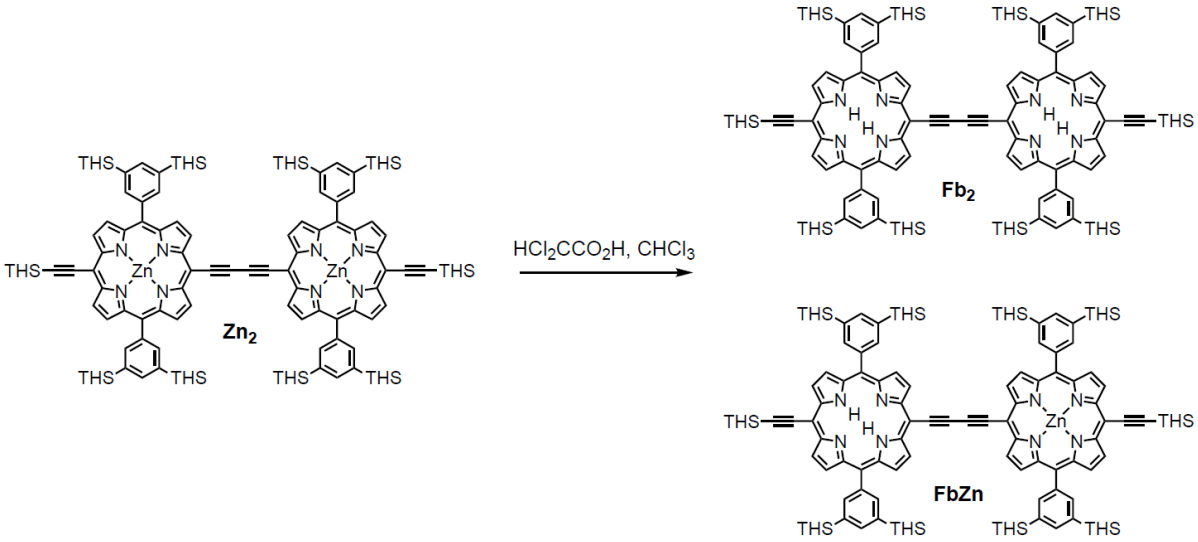

Dichloroacetic acid (1.3 mL, 16 mmol) was added dropwise to a solution of **Zn_2** (150 mg, 37.8 μmol) in $CHCl_3$ (40 mL). The solution was stirred at 20 °C for 2.5 h and monitored by TLC, then filtered through a short plug of silica gel eluting with $CHCl_3$ (with 1% pyridine). The product was purified by column chromatography on silica (eluting with petrol ether to petrol ether/dichloromethane 30:1). **Fb_2** (10 mg, 6.7%) and **ZnFb** (46 mg, 31%) were obtained successively as green solids, together with reisolated **Zn_2** (52 mg).

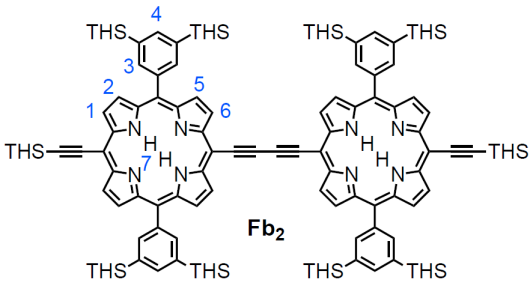

Fb_2: R_f = 0.88 (petrol ether/dichloromethane 15:1). **^{1}H-NMR** (400 MHz, $CDCl_3$): δ = 9.83 (4H, d, J = 4.8 Hz, H_6), 9.62 (4H, d, J = 4.8 Hz, H_1), 8.89 (4H, d, J = 4.8 Hz, H_5), 8.81 (4H, d, J = 4.8 Hz, H_2), 8.29 (8H, s, H_3), 8.02 (4H, s, H_4), 1.77–0.82 (390H, m, HTHS), −1.83 (4H, s, H_7).
MALDI-TOF: m/z = 3847.10 ($C_{252}H_{422}N_8Si_{10}$, M^+ requires 3844.10).
UV-vis-NIR (CH_2Cl_2): λ_{max}/nm (log ϵ) 448 (5.15), 484 (4.74), 540 (3.84), 627 (4.42), 735 (4.64).

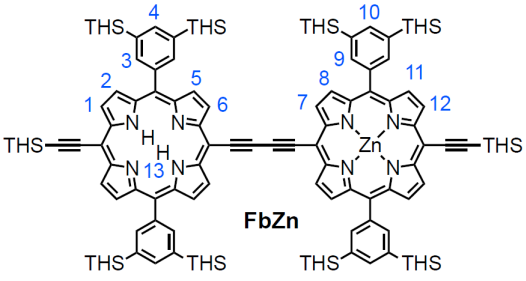

ZnFb: R_f = 0.72 (petrol ether/dichloromethane 10:1). **^{1}H-NMR** (400 MHz, $CDCl_3$): δ = 9.89 (2H, d, J = 4.7 Hz, H_7), 9.84 (2H, d, J = 4.8 Hz, H_6), 9.69 (2H, d, J = 4.7 Hz, H_{12}), 9.61 (2H, d, J = 4.8 Hz, H_1), 8.96 (2H, d, J = 4.7 Hz, H_8), 8.87 (4H, m, H5 and H_{11}), 8.80 (2H, d, J = 4.8 Hz, H_2), 8.28 (8H, d, J = 6.0 Hz, H_3 and H_9), 8.01 (4H, d, J = 5.3 Hz, H_4 and H_{10}) 1.78–0.86 (390H, m, HTHS), −1.82 (2H, s, H_{13}).
MALDI-TOF: m/z = 3910.28 ($C_{252}H_{420}N_8Si_{10}Zn$, M^+ requires 3908.02).
UV-vis-NIR (CH_2Cl_2): λ_{max}/nm (log ϵ) 450 (5.51), 485 (5.18), 547 (4.15), 594 (4.47), 648 (4.74), 725 (4.98).

Synthesis of PdFb and Pd_2

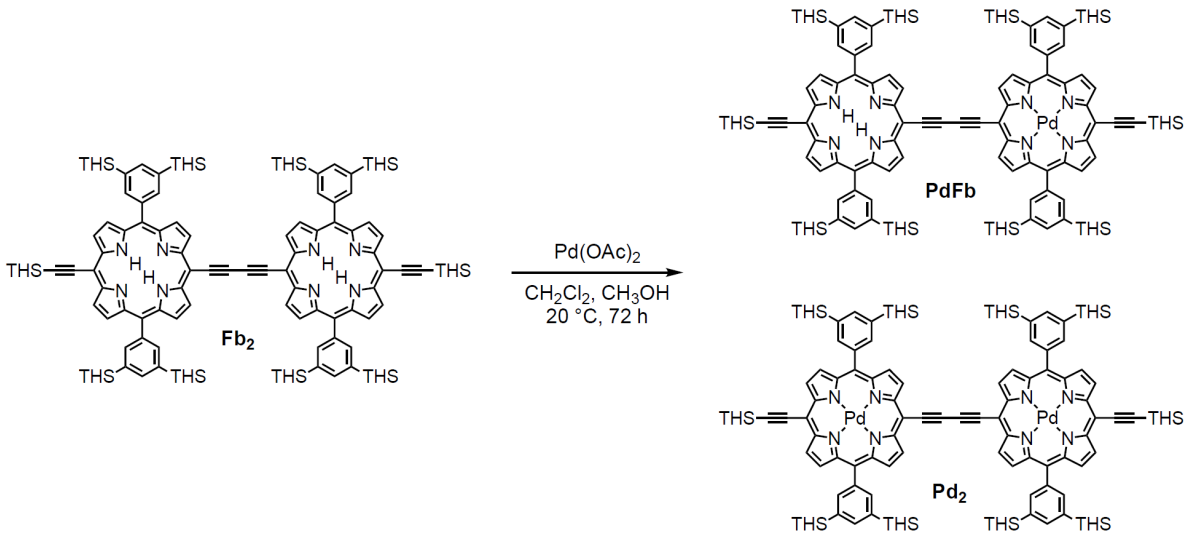

Fb_2 (33 mg, 8.58 μmol) and $Pd(OAc)_2$ (1.9 mg, 8.58 μmol) were dissolved in CH_2Cl_2 (16 mL) and CH_3OH (4 mL). The mixture was stirred at 20 °C for 3 days under an inert atmosphere. The solvent was evaporated and the residue was purified through column chromatography (silica gel, eluting with petrol ether). **PdFb** (7.8 mg, 23%) and **Pd_2** (5.6 mg, 15%) were obtained as green solids.

PdFb: R_f = 0.61 (petrol ether). **^{1}H-NMR** (400 MHz, CDCl3): δ = 9.74 (4H, m, H_6 and H_7), 9.53 (4H, m, H_1 and H_{12}), 8.81 (4H, m, H_5 and H_8), 8.73 (4H, m, H_2 and H_{11}), 8.21 (4H, s, H_3), 8.18 (4H, s, H_{10}), 7.94 (4H, s, H_4 and H_{10}), 1.70–0.62 (390H, m, HTHS), −1.92 (2H, s, H_{13}).
MALDI-TOF: m/z = 3951.32 ($C_{252}H_{420}N_8Si_{10}Pd$, M^+ requires 3948.99).
UV-vis-NIR (CH_2Cl_2): λ_{max}/nm (log ϵ) 448 (5.78), 477 (5.53), 609 (5.08), 635 (5.12), 712 (5.23).

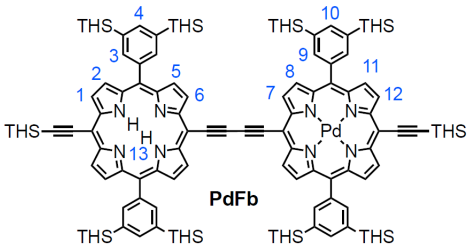

Pd_2: R_f = 0.90 (petrol ether). **^{1}H-NMR** (400 MHz, CDCl3): δ = 9.81 (4H, d, J = 4.9 Hz, H_6), 9.65 (4H, d, J = 4.8 Hz, H_1), 8.90 (4H, d, J = 4.9 Hz, H_5), 8.83 (4H, d, J =4.8 Hz, H_2), 8.26 (8H, s, H_3), 8.02 (4H, s, H_4), 1.54–0.87 (390H, m, HTHS).
MALDI-TOF: m/z = 4056.27 ($C_{252}H_{418}N_8Si_{10}Pd_2$, M^+ requires 4052.88).
UV-vis-NIR (CH_2Cl_2):λ_{max}/nm (log ϵ) 448 (5.43), 472 (5.32), 549 (4.42), 610 (4.84), 660 (5.04).

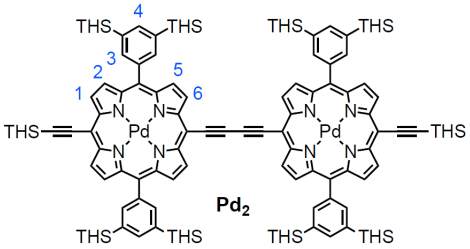

Synthesis of PdZn

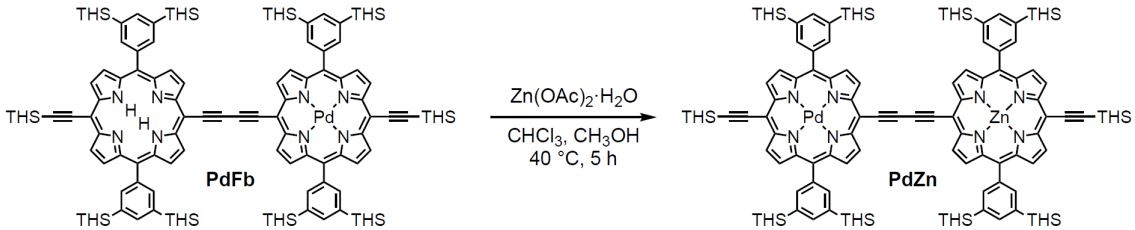

PdFb (7.8 mg, 19.7 μmol) and $Zn(OAc)_2 \cdot H_2O$ (4.3 mg, 1.97 μmol) were dissolved in $CHCl_3$ (10 mL) and CH_3OH (3 mL). The mixture was monitored by TLC and stirred at 40°C for 5 h. Then the mixture was filtered through a short plug of silica gel eluting with CHCl3 (with 1% pyridine). **PdZn**(7.9 mg, 100%) was obtained as a green solid.

PdZn: R_f = 0.53 (petrol ether). **^{1}H-NMR** (400 MHz, $CDCl_3$): δ = 9.87 (2H, d, J = 4.6 Hz, H_7), 9.81 (2H, d, J = 4.8 Hz, H_6), 9.68 (2H, d, J = 4.6 Hz, H_{12}), 9.59 (2H, d, J = 4.8 Hz, H_1), 8.95 (2H, d, J = 4.6 Hz, H_8), 8.86 (4H, m, H_5 and H_{11}), 8.80 (2H, d, J = 4.8 Hz, H_2), 8.26 (8H, d, J = 5.1 Hz, H_3 and H_9), 8.01 (4H, d, J = 5.1 Hz, H_4 and H_{10}), 2.05–0.70 (390H, m, HTHS).
MALDI-TOF: m/z = 4015.27 ($C_{252}H_{418}N_8Si_{10}PdZn$, M^+ requires 4011.90).
UV-vis-NIR (CH_2Cl_2): λ_{max}/nm (log ϵ) 451 (5.60), 479 (5.40), 553 (4.44), 595 (4.65), 686 (5.10).

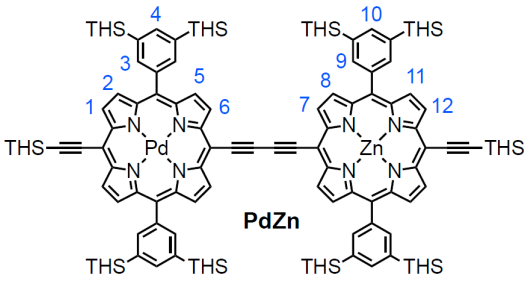

1.3 Synthesis of porphyrin oligomers

Palladium(II) metallated porphyrin oligomers **Pd$_N$** (N = 3, 4, 5, 6 and 7), were prepared from the zinc complexes **Zn$_N$** using the same procedures detailed above for the dimers, by analogy with the reported procedure for synthesis of platinum(II) metallated oligomers.[3]

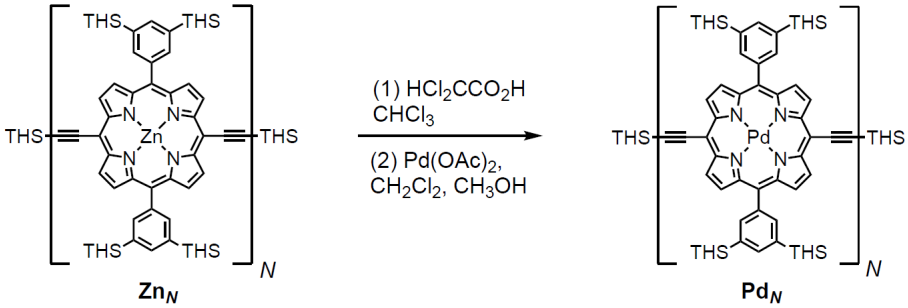

1.4 UV-vis absorption spectra

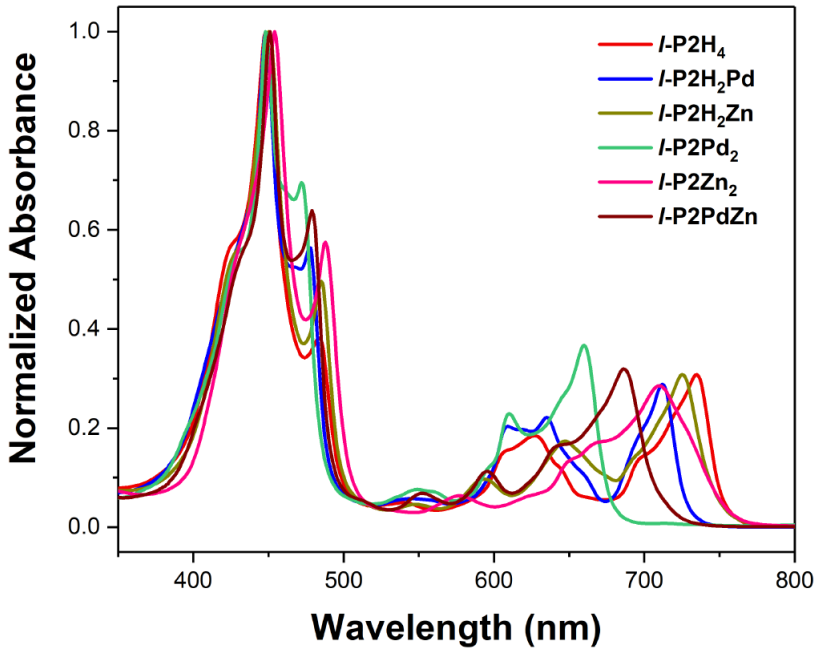

Figure S1: The normalized UV-vis-NIR spectra of dimers (concentration $\approx$ 1 μM, CH_2Cl_2, 25°C).

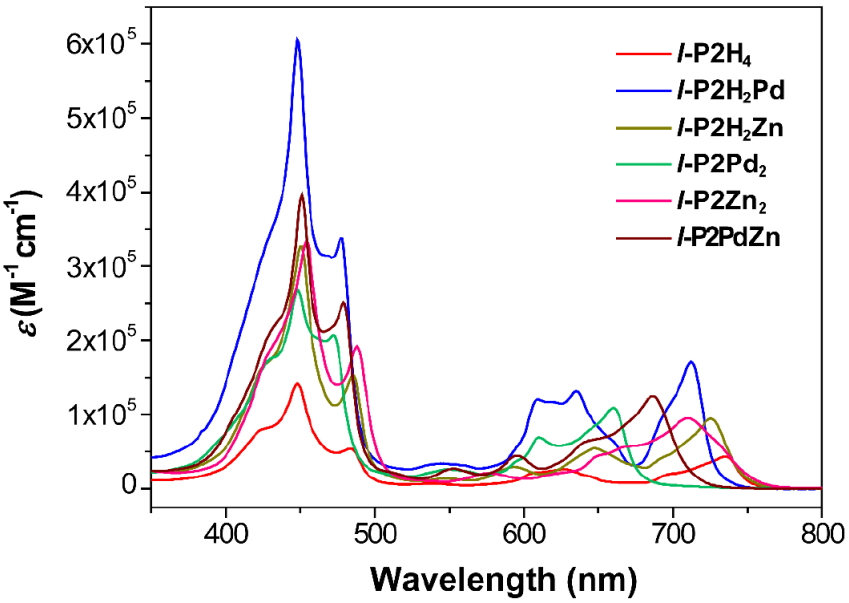

Figure S2: The molar absorption coefficient vs. wavelength UV-vis-NIR spectra of dimers (concentration $\approx$ 1 μM, CH_2Cl_2, 25°C).

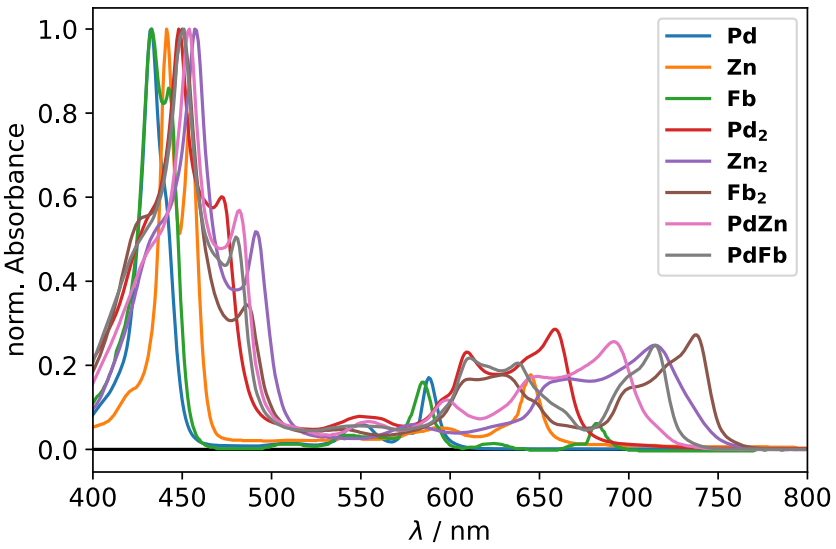

Figure S3: UV-vis absorption spectra of all the systems investigated in the main text (concentration $\approx$ 1 μM, toluene, 25°C).

1.5 ^{1}H-NMR spectra

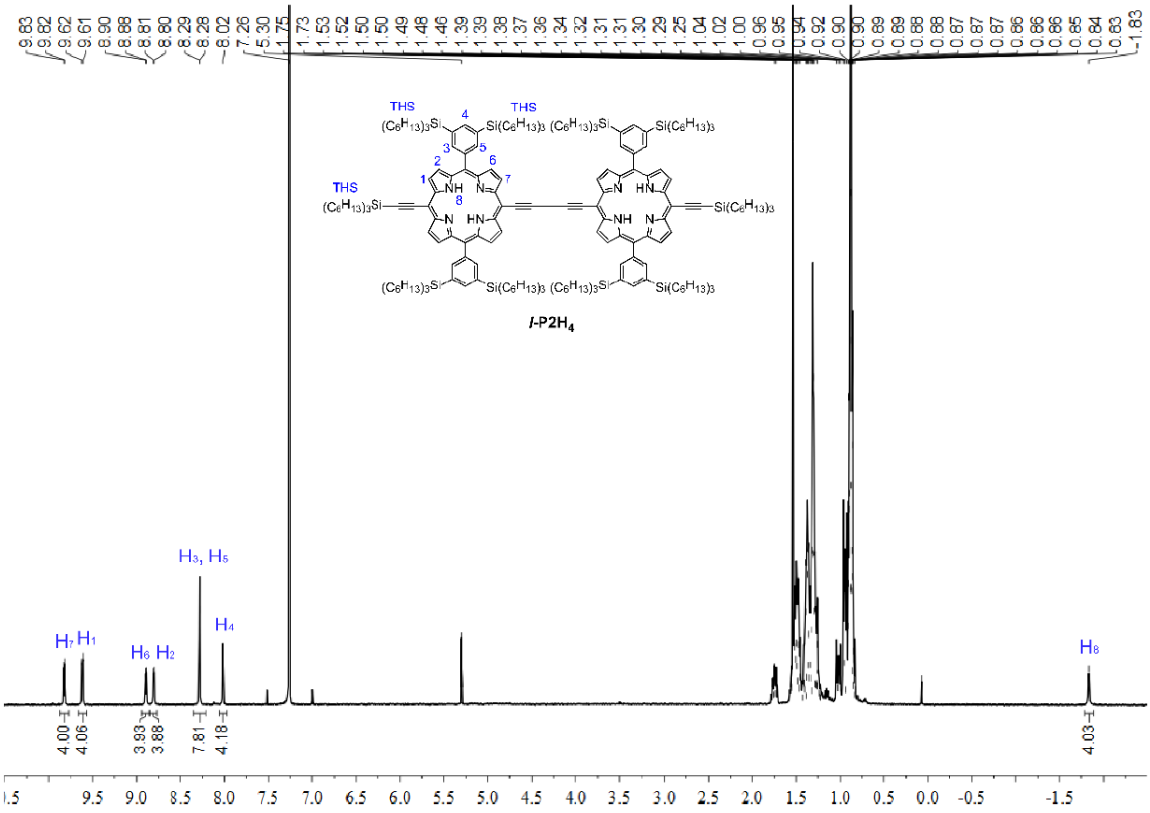

Figure S4: ^{1}H-NMR spectrum of **Fb$_2$** (400 MHz, $CDCl_3$).

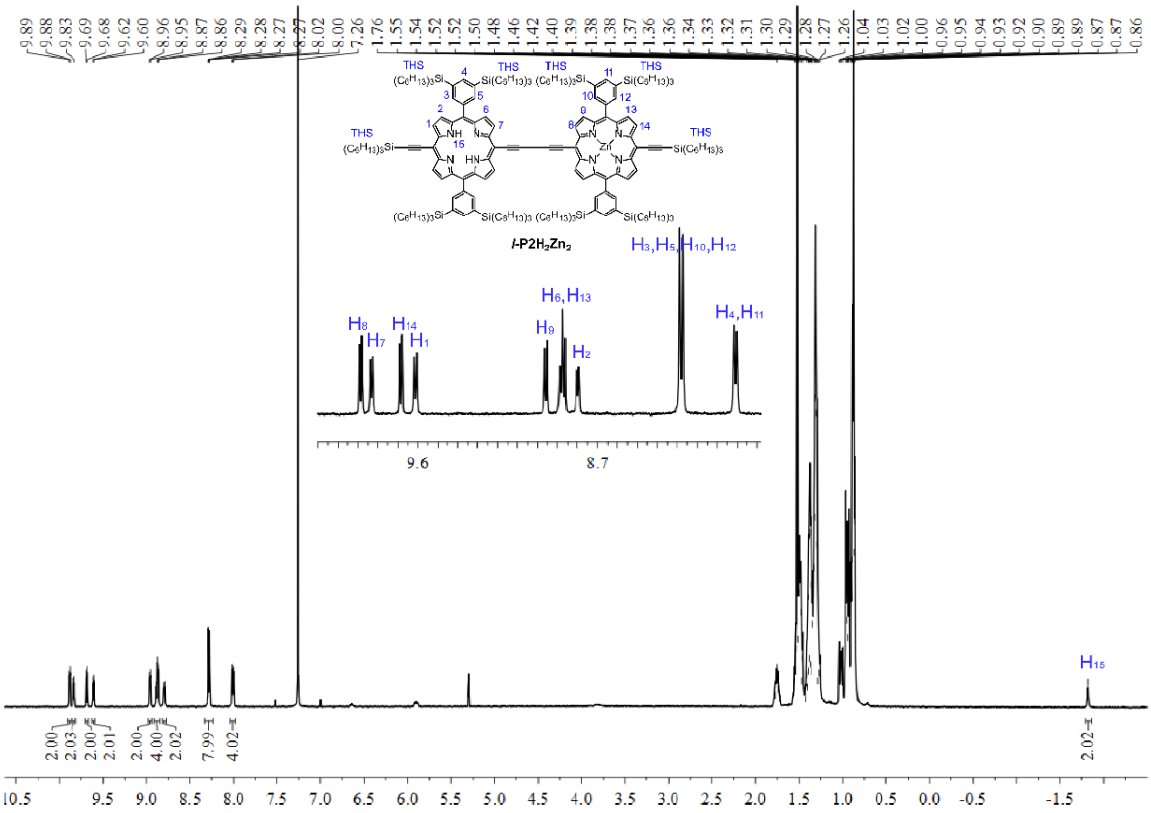

Figure S5: ^{1}H-NMR spectrum of **ZnFb** (400 MHz, $CDCl_3$).

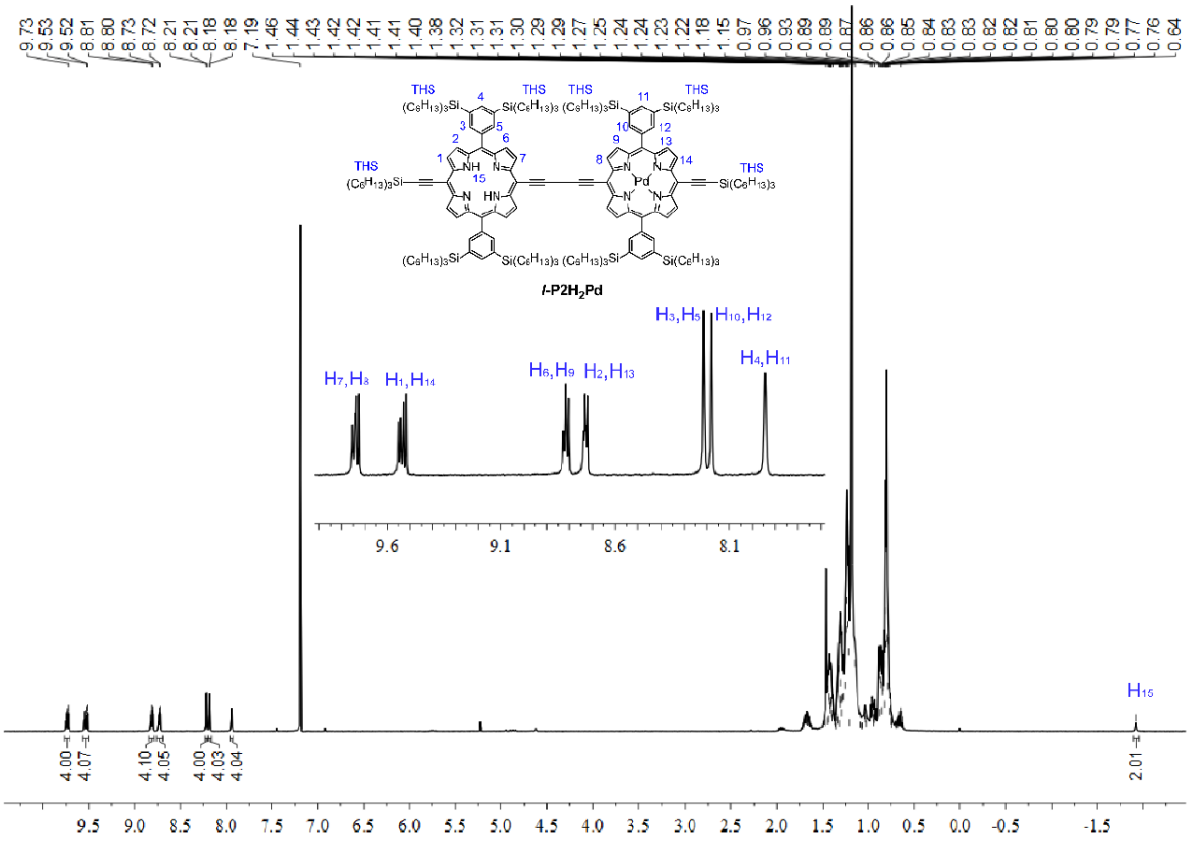

Figure S6: ^{1}H-NMR spectrum of **PdFb** (400 MHz, $CDCl_3$).

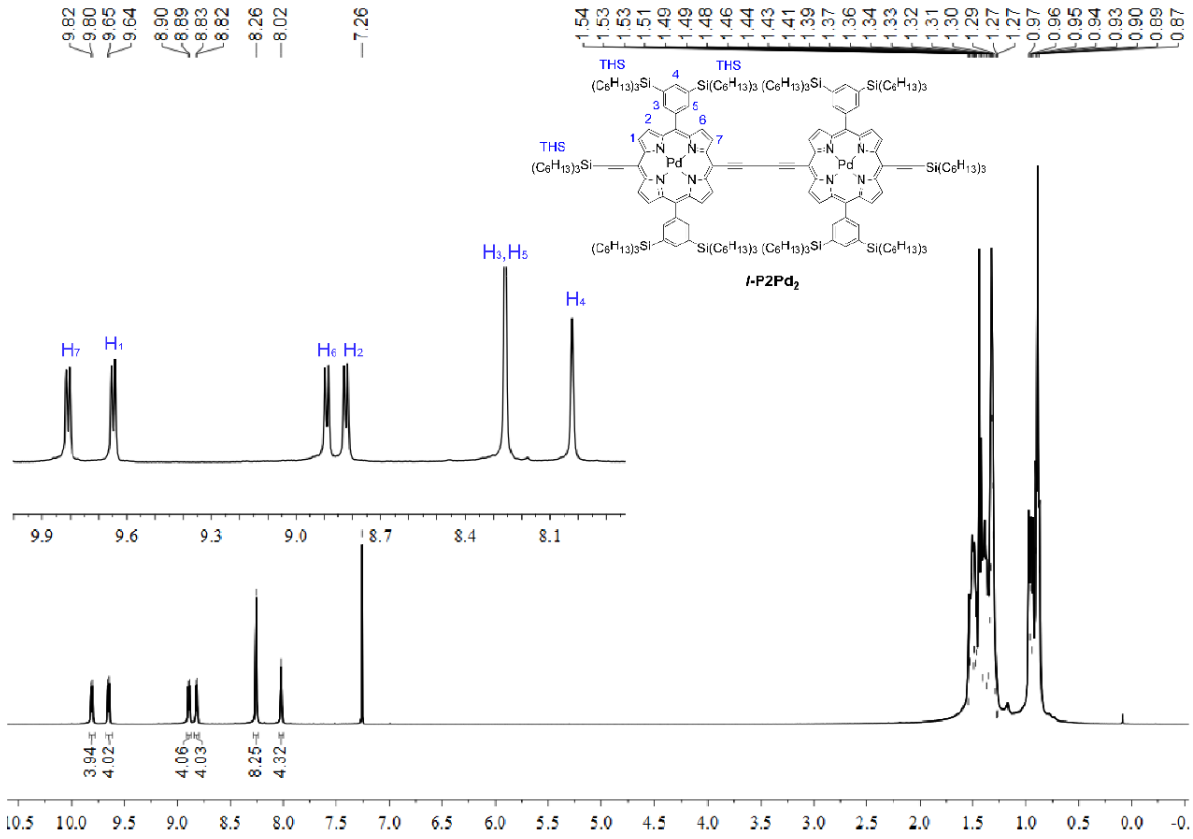

Figure S7: ^{1}H-NMR spectrum of **Pd_2** (400 MHz, $CDCl_3$).

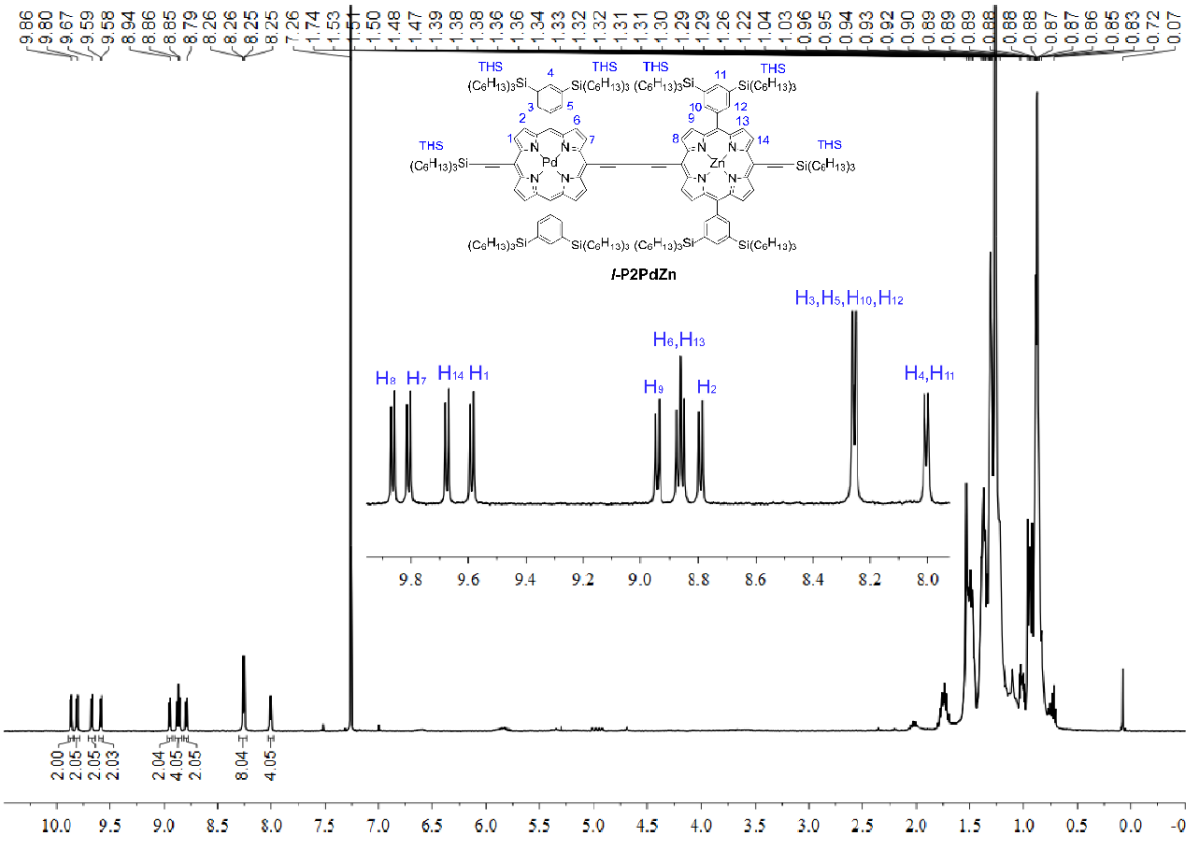

Figure S8: ^{1}H-NMR spectrum of **PdZn** (400 MHz, $CDCl_3$).

1.6 MALDI-TOF spectra

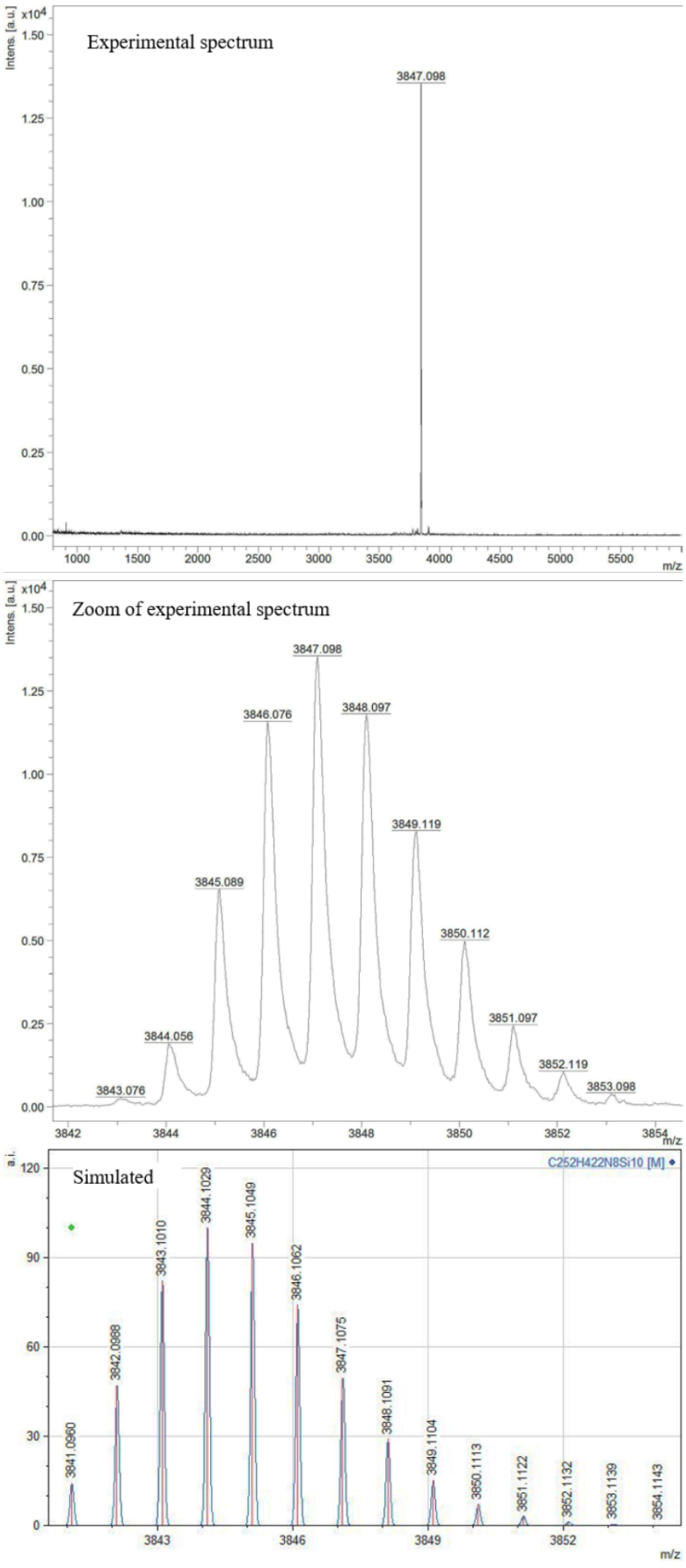

Figure S9: MALDI-TOF of $\mathbf{Fb_2}$.

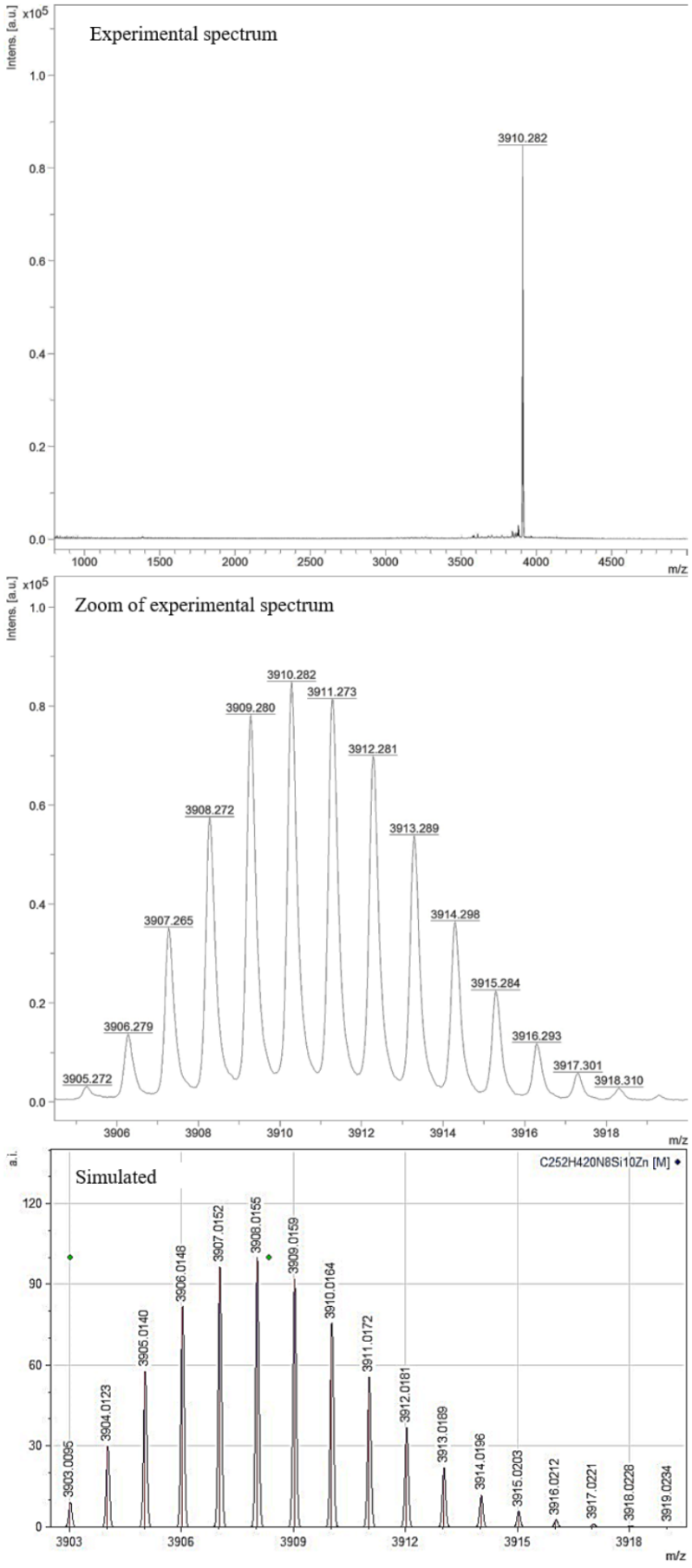

Figure S10: MALDI-TOF of **ZnFb**.

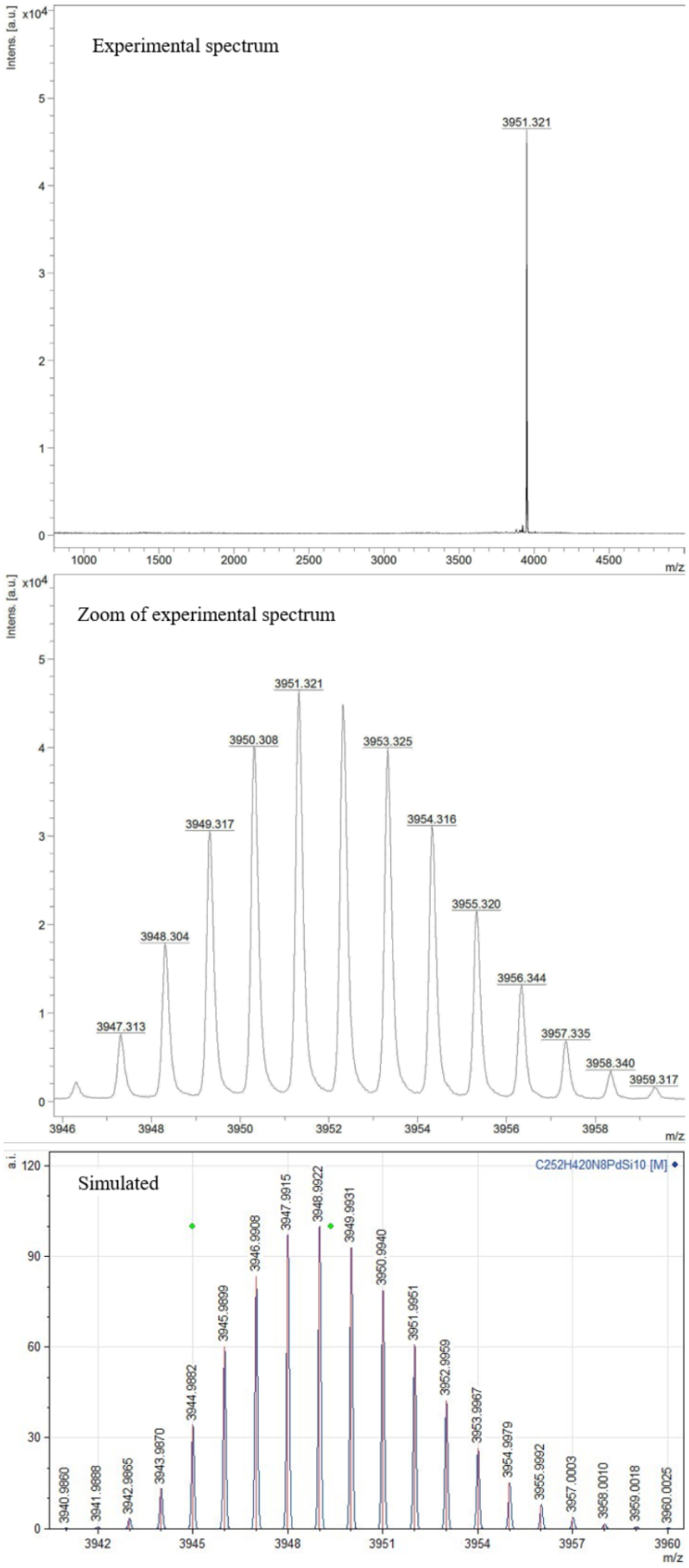

Figure S11: MALDI-TOF of **PdFb**.

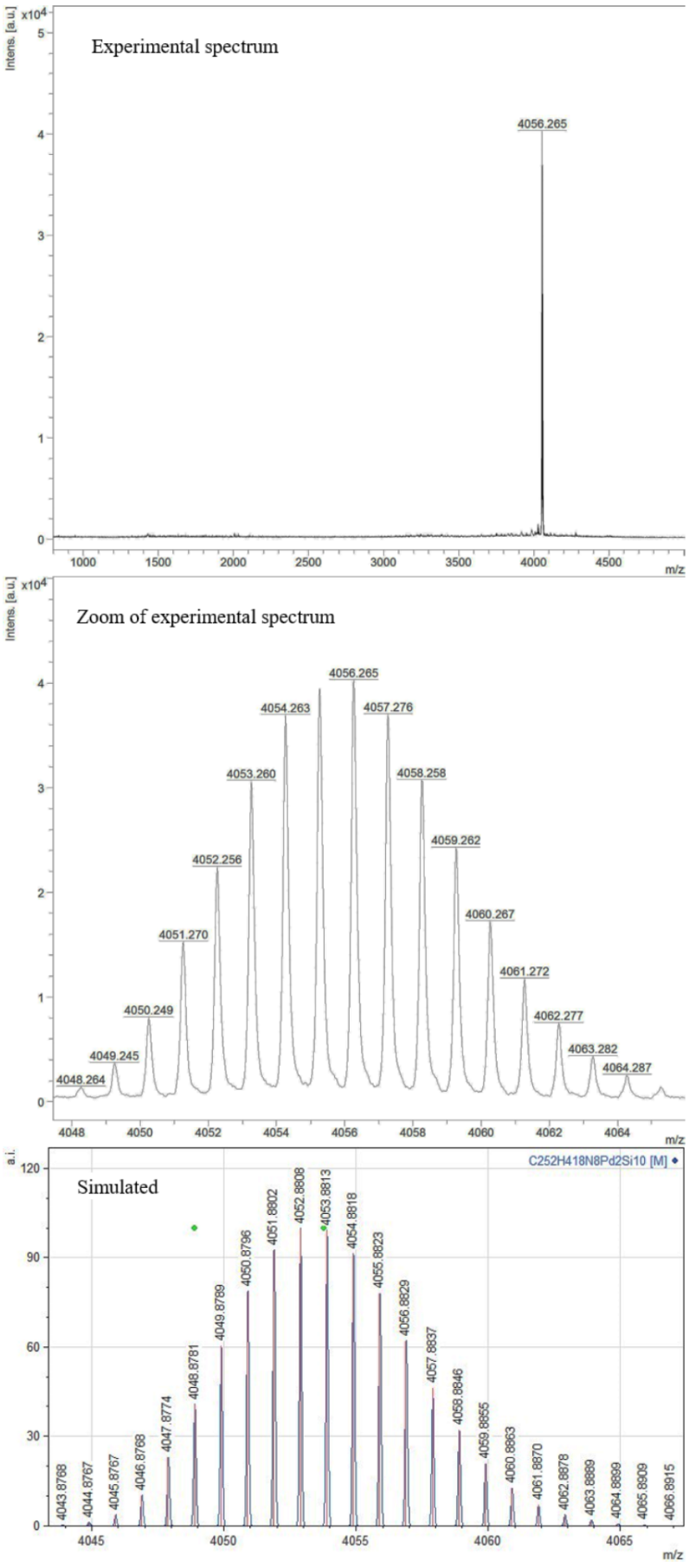

Figure S12: MALDI-TOF of $\mathbf{Pd_2}$.

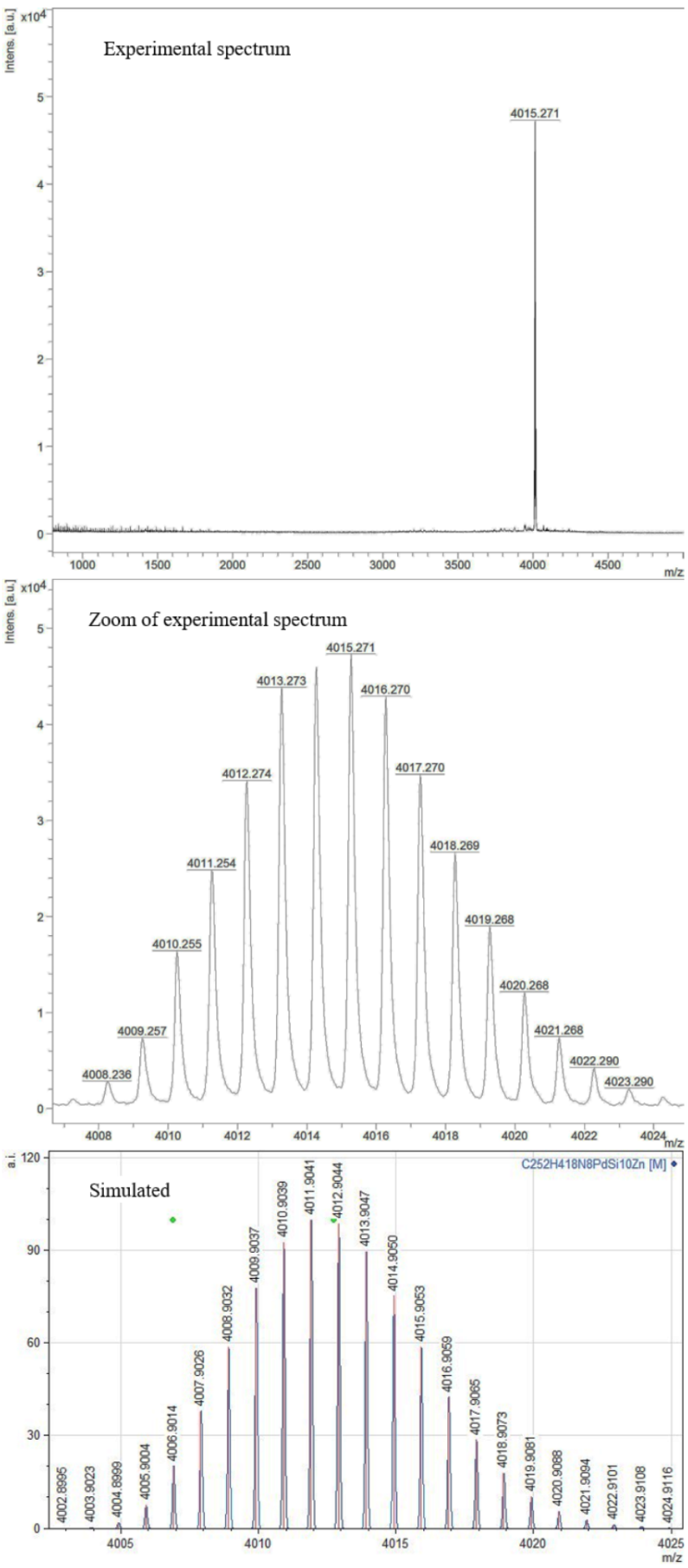

Figure S13: MALDI-TOF of **PdZn**.

2 X/W-band trESR on $\mathbf{Pd}_{n=1\rightarrow 7}$

Experimental details. The samples were prepared to a concentration of ca. 200 μM using 2-methyl-tetrahydrofuran for the X-band measurements and toluene for the W-band data. None of the EPR spectra displayed any signifcant differences at X-band in either solvent. Unless otherwise stated, the trESR spectra were recorded at 20 K using a Bruker Elexsys E680 spectrometer with an EN 4118X-MD4-W1 resonator for X-band and a EN600-1021H TeraFlex ENDOR resonator for W-band. A 3-300 kHz bandpass filter from Stanford Research Systems was used at W-band. The laser light was directed through the optical window of the cryostat at X-band and through a fibre optic coupled to the top of the sample tube at W-band. Laser excitation was performed with depolarised light at 532 nm using an Opotek Opolette HE 355 LD optical parametric oscillator pumped by the third harmonic of a Nd:YAG laser. The excitation energy was ca. 2 mJ at X-band and 0.5 mJ at W-band at a repetition rate of 20 Hz.

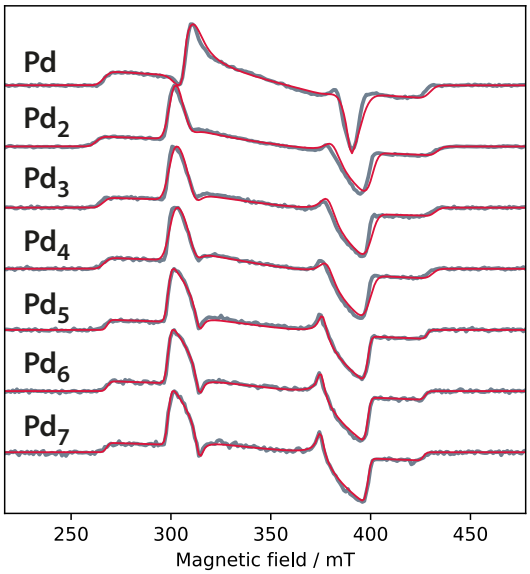

Figure S14: Experimental (solid black lines) and simulated (red lines) trESR spectra of the $\mathbf{Pd}_{n=1\rightarrow 7}$ systems acquired at X-band. For the systems up to the tetramer the simulations are a result of global fitting of X- and W-band data. The data in this figure were acquired using the methodology described in the main text.

System	D / MHz	λ	$\mathbf{P} = (P_x, P_y, P_z)$
Pd	−2289	0.00	(0.00, 1.00, 0.00)
$\mathbf{Pd_2}$	−2362	0.06	(0.01, 0.99, 0.00)
$\mathbf{Pd_3}$	−2322	0.07	(0.05, 0.95, 0.00)
$\mathbf{Pd_4}$	−2282	0.07	(0.03, 0.97, 0.00)
$\mathbf{Pd_5}$	−2242	0.08	(0.00, 0.95, 0.05)
$\mathbf{Pd_6}$	−2229	0.08	(0.00, 0.91, 0.07)
$\mathbf{Pd_7}$	−2232	0.06	(0.00, 0.89, 0.11)

Table 1: Best fit values of the ZFS parameters (D and λ) and relative sub-level populations (the population vector, **P**) for the series of porphyrin oligomers. For the oligomers up to the tetramer, the parameters were obtained by global fitting of the X- and W-band data (figure S15). For the pentamer, hexamer, and heptamer, the parameters are obtained only from the X-band data and simulations in figure S14. These simulation parameters are not exactly identical to the ones reported in the main text for **Pd** and $\mathbf{Pd_2}$ because they were obtained by global fitting whereas only the X-band simulation results are shown in the main text.

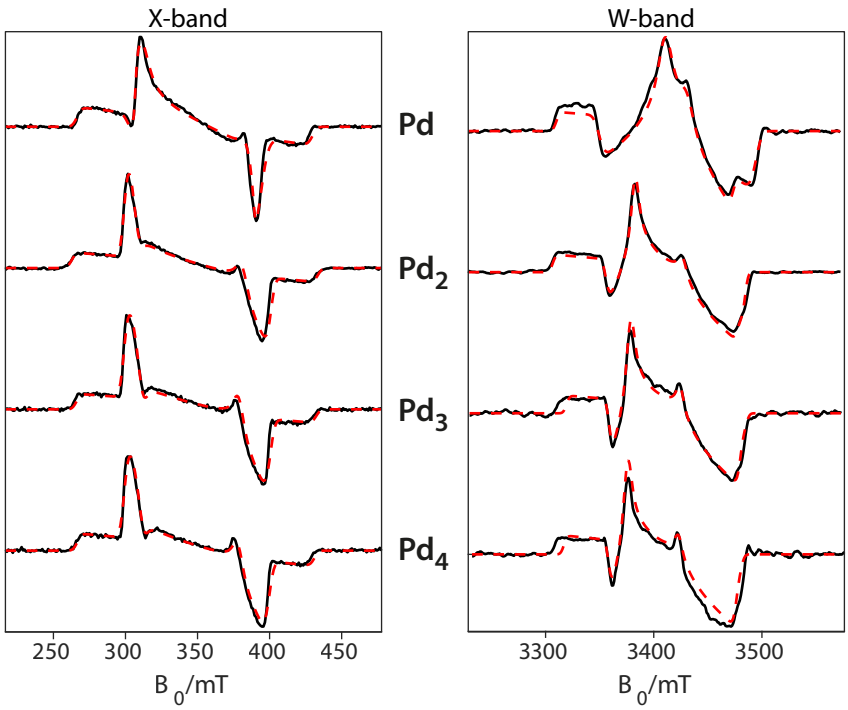

Figure S15: Experimental (solid black lines) and simulated (dashed red lines) trESR spectra of the **Pd** and $\mathbf{Pd}_{2 \leq n \leq 4}$ systems acquired at X-band and W-band. The simulations are a result of global fitting using EasySpin.[4] The X-band data was acquired as per the details provided in the main text. The W-band acquisition details are given in this section.

3 ENDOR on $\mathbf{Pd_{n=1\rightarrow5}}$

Experimental details. All ENDOR spectra reported in figure S16 were acquired using the exact same procedure as explained in the 'Theory and methods' section in the main text.
Discussion. The conservation of the spin density delocalisation in $\mathbf{Pd_2}$ relative to $\mathbf{Zn_2}$ remains a feature of the entire series of linear palladium oligomers as can be seem from the ENDOR data in figure S16. In particular, the spectra recorded at the XY^- field position indicate that the largest hyperfine coupling is approximately halved in all the $\mathbf{Pd}_{n\geq2}$ oligomers relative to **Pd**. The slight increase of the largest coupling in $\mathbf{Pd_3}$ relative to $\mathbf{Pd_2}$ indicates that the spin density is slightly more localised on the central porphyrin unit whilst simultaneously leaking onto the peripheral fragments. Beyond $\mathbf{Pd_3}$, there is virtually no change in the magnitudes of the hyperfine couplings, indicating that the spin density does not delocalise any further than approximately 2-3 units. The exact same observations were reported for the $\mathbf{Zn_n}$ series.[5] Furthermore, as pointed out in the caption of figure S16, the conserved position of the hyperfine peaks relative to the Larmor peaks confirms that the orientation of the **D**-tensor is the same throughout the $\mathbf{Pd_n}$ series.
The SOC contribution to **D** is clearly persistent throughout the entire $\mathbf{Pd_n}$ series, apart from the apparent reduction from monomer to dimer. This is also reflected in the spin polarisation of the series (table 1), which remains persistently in the out-of-plane direction (within simulation error). Hence, incorporating Pd^{2+} into all the units of a linear porphyrin chain conserves spin delocalisation (relative to the free-base and Zn^{2+} analogues) and promotes a stronger out-of-plane spin polarisation.

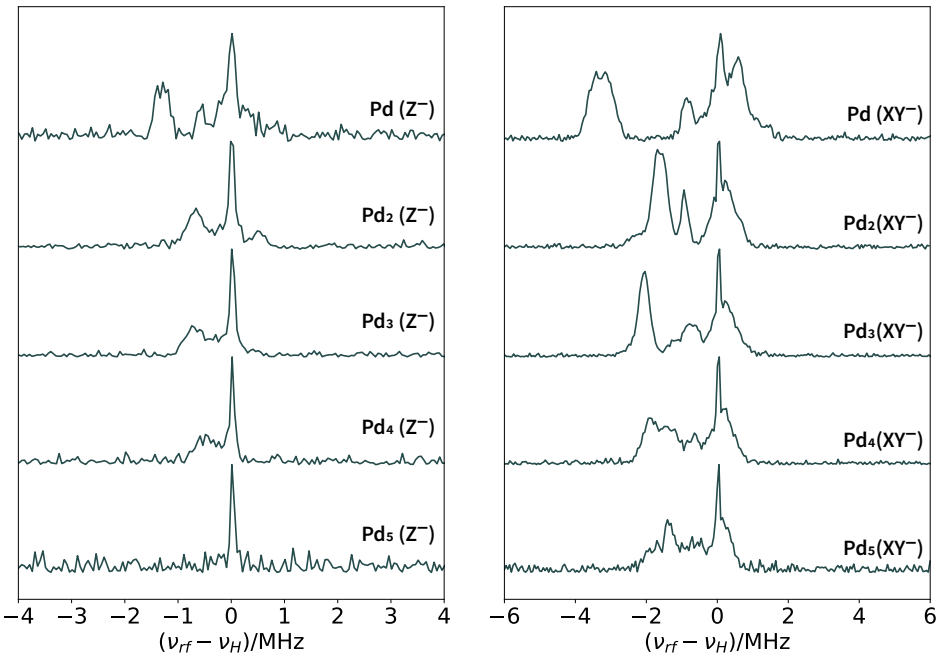

Figure S16: Mims ^{1}H-ENDOR spectra of the $\mathbf{Pd_n}$ systems up to the pentamer. The spectra were recorded analogously to the ENDOR data in the main text at the field positions corresponding to the Z^- and XY^- transitions in the ESR spectra. The magnitude of the largest hyperfine coupling is smaller in all the oligomers beyond the monomer by a factor of approximately two. This indicates that the spin density is delocalised over approximately 2-3 units in the longer oligomers, akin to the zinc porphyrin oligomers.[2] Since all these ENDOR spectra are acquired at approximately the same field position and the hyperfine peaks do not swap to the other side of the Larmor peak across the entire series, we may conclude that the orientation of the **D**-tensor is the same throughout the series.

4 MPS on Pd_2

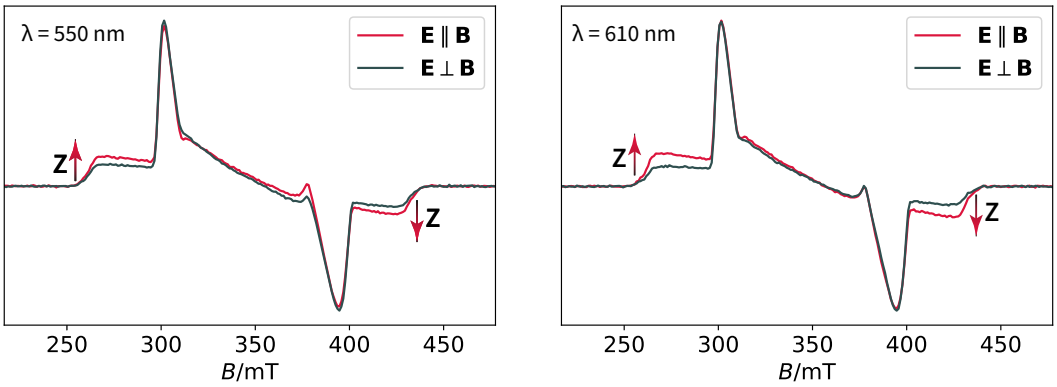

Figure S17: MPS results on the **Pd_2** system. The MPS effect is weak for this system at both of the indicated wavelengths. Unfortunately, no other position in the absorption spectrum yielded a more pronounced effect than what is observed here at 550 and 610 nm. The data is consistent with a negative D-value for the **Pd_2** system. When **E** ∥ **B**, the Z canonical orientations of the **D** tensor are enhanced whereas the XY positions remain effectively unchanged (if not slightly diminished). This indicates that the D_z axis is reasonably close to the optical transition dipole moment, $\boldsymbol{\tau}$, and hence, $D < 0$.

5 Wavelength and time (in)dependence of the PdFb trESR spectra

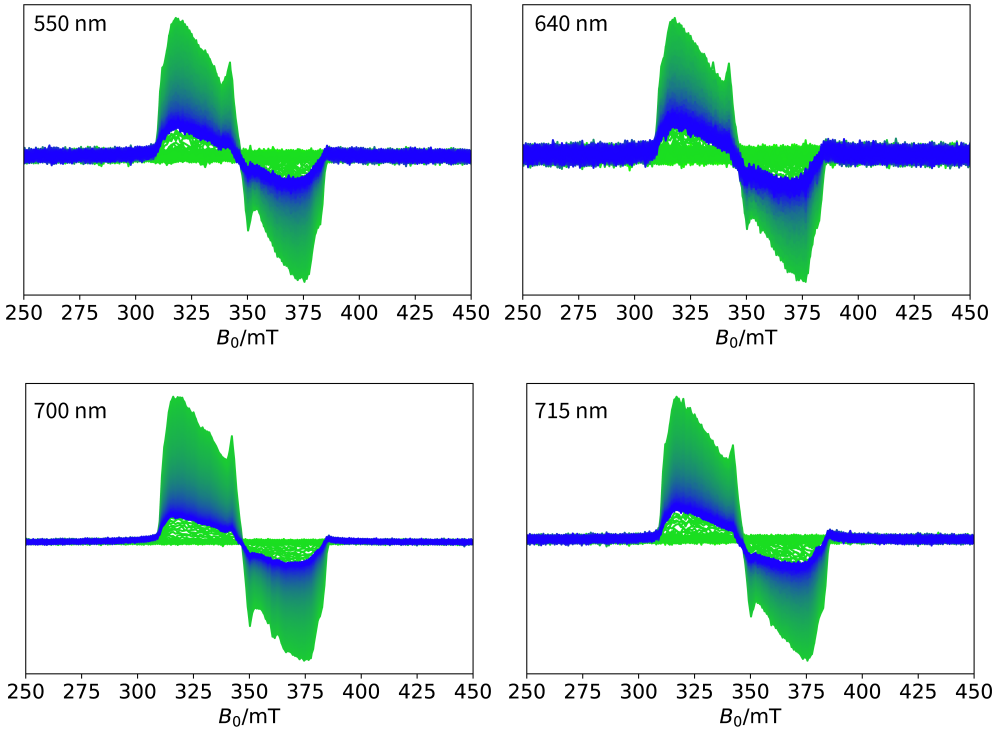

Figure S18: Time evolution over a range of 8 μs of the trESR spectra of the **PdFb** system measured by excitation at the indicated wavelengths. All other acquisition parameters are analogous to the X-band trESR data in the main text. The colourmap is as follows: early times are predominantly green and as time progresses the lines become predominantly blue. These data illustrates that the overall shape of the ESR spectrum is conserved as a function of time regardless of excitation wavelength.

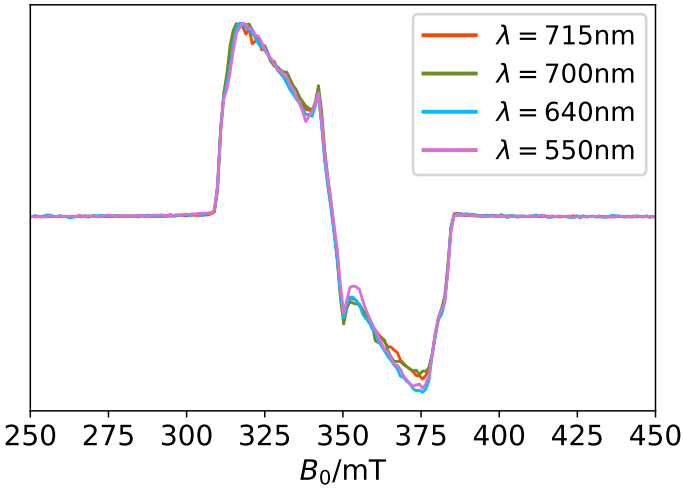

Figure S19: Time averaged trESR spectra of **PdFb** obtained over a range of 800 ns after the maximum signal in time-domain (figure S18). There is no change in the ZFS and spin polarisation as a function of wavelength. In other words, the same final triplet state is observed regardless of where photoexcitation takes place in the absorption spectrum.

6 CASSCF spin densities of Fb, Zn, and Pd

Computational details. The spin densities depicted in figure S20 were obtained using ORCA.[6] An initial geometry optimisation using DFT was performed with the BY3LYP functional and the def2-SVP basis for C, H, N, and def2-TZVP for Zn and Pd. The DFT wavefunction was then used for the CASSCF calculation with an active space of 4 electrons and 4 orbitals. The CASSCF calculation was performed on a triplet block comprised of four electronic states. The displayed spin densities are for the lowest energy triplet state.

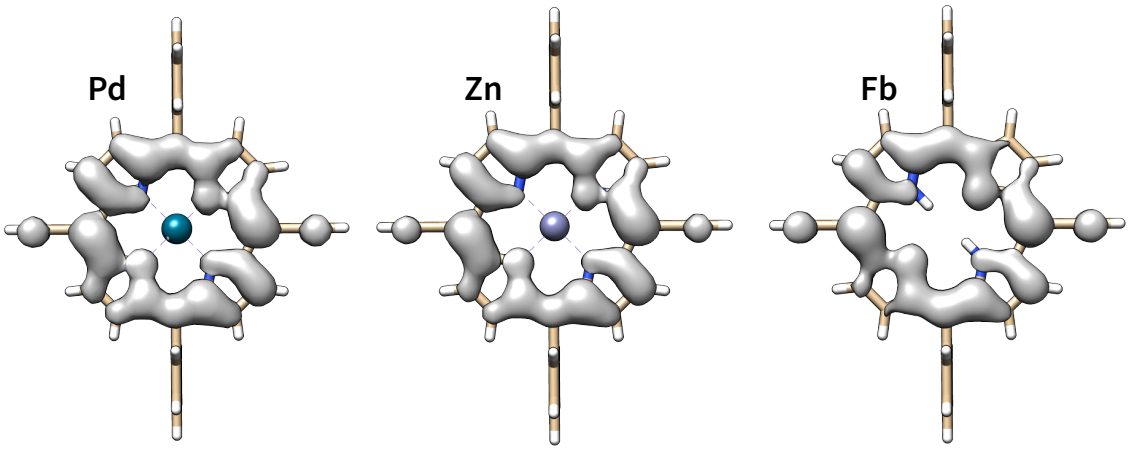

Figure S20: Spin densities of **Pd**, **Zn**, and **Fb** obtained from a CASSCF calculation with an active space of four electrons and four orbitals. The dipolar contribution to the *D*-value obtained from these spin densities are (in MHz): +918, +910, and +1027 for **Pd**, **Zn**, and **Fb**, respectively. The latter two values are in excellent agreement with the experimental values reported in the main text (which validates the supposition that the *D*-value of **Zn** and **Fb** is purely dipolar in origin). These results illustrate that the spin density distribution in the three monomer systems is approximately the same. The importance of this result is to provide a theoretical basis for the assumption made in the discussion of the ENDOR data in the main text, *i.e.* that the hyperfine tensors in the the three systems are approximately the same and hence, the orientation of **D** in **Pd** can be determined from ENDOR.

7 An exploration of $4! = 24$ possible energetic orderings of the excited states

This section expands the discussion associated with figure 5 of the main text to all the remaining orderings of the four excited states. The purpose of the discussion is to shed light on the SOC contribution to the fine-structure and spin polarisation of the **Pd** system. In the main text, the following ordering was explored: ${}^3B_{2u} - {}^3B_{3u} - {}^1B_{2u} - {}^1B_{2u}$, in order of increasing energy from left to right. The following assumptions are made throughout:

(*a*) ***Symmetry.*** The system blongs to the D_{2h} point group. The three components of the SOC operator transform as $B_{1g} \rightarrow R_z$, $B_{2g} \rightarrow R_y$, $B_{3g} \rightarrow R_x$. The subscripts x, y, z refer to the molecular axes.

(*b*) ***Initial singlet state.***

(*c*) ***Rapid ergodicity.*** The photophysical cascade initiated by light excitation is energetically downhill until the final triplet state is formed. This is the triplet state detected in the trESR data. No thermally activated, or otherwise, uphill processes are considered. No intermediates are detectable.

(*d*) ***Total spin conserving processes are fastest.*** In other words, the rate of internal conversion (IC) is larger than ISC. This assumption is not necessary; it does, however, simplify the discussion.

(*e*) ***Conservation of the spin polarisation during IC.*** Strictly speaking, this is not, in fact, an assumption in the framework of these particular excited states. The SOC interaction may mediate the conversion between the two triplets, ${}^3B_{3u}$ and ${}^3B_{2u}$, only via the z-component. For IC between the singlets, this statement is irrelevant.

(*f*) ***Closest electronic state contributes to*** **D.** In other words, the second-order pertubational correction to the **D**-tensor is truncated to the term closest in energy. Although not discussed in the main text, singlet states may also contribute to **D**.[7]

(*g*) ***Closest triplet state contributes to*** **g.** There is no singlet-triplet contribution to the **g**-tensor.[7]

Regarding the 24 possible orderings: 12 will correspond to a singlet state being the lowest energy excited state. Such orderings are irrelavant because they would not lead to a triplet state detectable by ESR, by the ergodicity assumption.
The remaining 12 orderings, with a lowest triplet state, have ${}^3B_{2u}$ either higher or lower than ${}^3B_{3u}$. Supposing ${}^3B_{3u}$ were the trESR detected triplet, only 6 orderings need to be considered. This ${}^3B_{3u}$ state must have been formed either by ISC from a ${}^1B_{2u}$ via the z-component of SOC or by a polarisation conserving IC step from ${}^3B_{2u}$ which, in turn, could only have emerged by ISC from ${}^1B_{3u}$. Both ISC events are promoted by the z-component of SOC, and the IC step does not change spin polarisation. Although not necessary, for the ISC-IC scenario, we may now rule out (from the remaining 6) the 2 orderings which have ${}^3B_{2u}$ as the highest energy excited state because it can never be reached due to ergodicity. Overall, the only possible outcome is an out-of-plane spin polarisation. The arguments are trivially the same for the case when ${}^3B_{2u}$ is lowest in energy.
Assumptions *(f)* and *(g)* immediately imply that the orientations of **g** and **D** are independent of the energetic ordering because either tensor will always originate in the mixing of a B_{2u} term with a B_{3u} term, exactly as already described in the main text.

References

[1] Ferdinand C Grozema, Coralie Houarner-Rassin, Paulette Prins, Laurens DA Siebbeles, and Harry L Anderson. Supramolecular control of charge transport in molecular wires. *Journal of the American Chemical Society*, 129(44):13370–13371, 2007.

[2] C. E. Tait, P. Neuhaus, M. D. Peeks, H. L. Anderson, and C. R. Timmel. Transient epr reveals triplet state delocalization in a series of cyclic and linear π-conjugated porphyrin oligomers. *Journal of the American Chemical Society*, 137(25):8284–8293, 2015.

[3] Ja Kyung Lee, Ibrahim Bulut, Michel Rickhaus, Yuewen Sheng, Xiang Li, Grace GD Han, G Andrew D Briggs, Harry L Anderson, and Jamie H Warner. Metal atom markers for imaging epitaxial molecular self-assembly on graphene by scanning transmission electron microscopy. *ACS nano*, 13(6):7252–7260, 2019.

[4] S. Stoll and A. Schweiger. Easyspin, a comprehensive software package for spectral simulation and analysis in epr. *Journal of magnetic resonance*, 178(1):42–55, 2006.

[5] C. E. Tait, P. Neuhaus, H. L. Anderson, and C. R. Timmel. Triplet state delocalization in a conjugated porphyrin dimer probed by transient electron paramagnetic resonance techniques. *Journal of the American Chemical Society*, 137(20):6670–6679, 2015.

[6] F. Neese. The orca program system. *Wiley Interdisciplinary Reviews: Computational Molecular Science*, 2(1): 73–78, 2012.

[7] F. Neese and E. I. Solomon. Calculation of zero-field splittings, g-values, and the relativistic nephelauxetic effect in transition metal complexes. application to high-spin ferric complexes. *Inorganic chemistry*, 37(26): 6568–6582, 1998.